Cryo-EM Structures of the Actin:Tropomyosin Filament Reveal the Mechanism for the Transition from C- to M-State

Duncan R. Sousa[1,2], **Scott M. Stagg**[3] and **M. Elizabeth Stroupe**[1]

*1 - **Department of Biological Science and Institute of Molecular Biophysics,** Florida State University, 91 Chieftan Way, Tallahassee, FL 32306, USA*
*2 - **Department of Physiology and Biophysics,** Boston University School of Medicine, 72 East Concord Street, Boston, MA 02118-2526, USA*
*3 - **Department of Chemistry and Biochemistry and Institute of Molecular Biophysics,** Florida State University, 91 Chieftan Way, Tallahassee, FL 32306, USA*

***Correspondence to M. Elizabeth Stroupe:** 91 Chieftan Way, Tallahassee, FL 32306, USA. 91 Chieftan Way, Tallahassee, FL 32306, USA. mestroupe@bio.fsu.edu*
http://dx.doi.org/10.1016/j.jmb.2013.08.020
Edited by E. Nogales

Abstract

Tropomyosin (Tm) is a key factor in the molecular mechanisms that regulate the binding of myosin motors to actin filaments (F-Actins) in most eukaryotic cells. This regulation is achieved by the azimuthal repositioning of Tm along the actin (Ac):Tm:troponin (Tn) thin filament to block or expose myosin binding sites on Ac. In striated muscle, including involuntary cardiac muscle, Tm regulates muscle contraction by coupling Ca^{2+} binding to Tn with myosin binding to the thin filament. In smooth muscle, the switch is the posttranslational modification of the myosin. Depending on the activation state of Tn and the binding state of myosin, Tm can occupy the blocked, closed, or open position on Ac. Using native cryogenic 3DEM (three-dimensional electron microscopy), we have directly resolved and visualized cardiac and gizzard muscle Tm on filamentous Ac in the position that corresponds to the closed state. From the 8-Å-resolution structure of the reconstituted Ac:Tm filament formed with gizzard-derived Tm, we discuss two possible mechanisms for the transition from closed to open state and describe the role Tm plays in blocking myosin tight binding in the closed-state position.

Introduction

Striated and smooth actin:tropomyosin

Tropomyosin (Tm) is an important component in most actin filament (F-Actin) structures and is therefore essential to cell motility, morphology, organization, and structure (reviewed by Perry [1]). Different Tm isoforms are required for survival of organisms from yeast to humans: they play a critical role in muscle contraction as part of muscle thin filament and support F-Actin's diverse cellular function outside the context of muscle contraction (reviewed by Gunning et al. [2]).

High-molecular-weight (HMW) Tm is a 40-nm-long, dimeric coiled coil that cooperatively polymerizes end to end along the surface of F-Actin [3–8]. Striated and smooth muscle contain HMW Tm, where its coiled coil wraps continuously around F-Actin to form part of the thin filament that helps elicit voluntary and involuntary muscle contraction [8]. In addition, both cardiac and skeletal thin filaments from striated muscle contain troponin (Tn), a regulator that links muscle activation to cellular Ca^{2+} concentration [9]. Smooth muscle actin (Ac):Tm, such as that found in the gizzard, does not use Tn to control activity but relies on posttranslational modification of the myosin with which it interacts [10]. HMW Tm is 284 amino acids long and is strongly conserved between species, despite being expressed from multiple genes and multiple promoters, and as multiple splice isoforms (Fig. 1) [1,2,11].

Tm binds F-Actin and regulates muscle contraction

The sequence of amino acids in cardiac and gizzard Tm (and other HMW Tms) forms a pattern that determines how Tm binds F-Actin (Fig. 1a). A total of

41 sequential heptad repeats comprise the Tm α-helix that dimerizes as a coiled coil and then binds in a repeating pattern along the length of the F-Actin molecule [12]. The protein products from the α and β isoforms, the predominant forms found in cardiac (αα) or gizzard (αβ) tissue, are 72% identical, with the least conserved segment lying in the C-terminus of the protein (Fig. 1a). Those heptad repeats translate into seven pseudo-repeating units per dimer, marked by the coiled-coil crossover, that conform to the path of seven successive Ac monomers within one-half of the two-start F-Actin helix [13–15]. Strategically located alanines interspersed along the heptad repeats allow smooth, anisotropic bending of the long coiled coil, suggesting that Tm is preformed into a shape that is complementary to F-Actin's twist [12,16–19]. Further, this innate superhelical twist suggests that movement of Tm along one part of the Ac:Tm filament can propagate along the Tm polymer, promoting the cooperative nature of F-Actin regulation by Tm [20,21].

In muscles, the thin filament works with myosin-containing thick filaments to regulate muscle contraction [22–24]. Tm plays an integral role in this regulation by cooperatively regulating access of other Ac binding proteins onto the F-Actin surface. Specifically, striated muscle Tm and Tn alternatively inhibit, allow, or enhance myosin binding to F-Actin to control the myosin cross-bridge cycling in response to Ca^{2+} concentration and consequently relax or promote muscle contraction [25]. In this model, known as the three-state steric blocking model of muscle regulation, Tm can occupy three states that are defined biochemically and structurally: blocked, closed, and open [26,27]. Smooth muscle is proposed to work in a similar fashion, but posttranslational modification of myosin by myosin light chain kinase, regulated by the Ca^{2+}-binding calmodulin, performs a similar role to Tn/Ca^{2+} control of Tm position [28,29].

Blocked, closed, and open states are defined biochemically and structurally

In the blocked state ("B"), myosin binding to F-Actin is inhibited by Tm:Tn – Ca^{2+} (Tm:Tn minus Ca^{2+} will be designated Tm:Tn – Ca^{2+} throughout the article). According to the structural interpretation of the B-state inferred from negatively stained EM images of Ac:Tm and Ac:Tm:Tn, Tm is pinned in place by Ca^{2+}-free Tn such that Tm covers the myosin binding site on Ac [30]. In solution, the B-state is occupied only in Ca^{2+}-free Tn-containing filaments and never in the Tn-free Ac:Tm filament or in the presence of Tn and Ca^{2+} [26]. Depending on the isoform, however, the Tm position that corresponds to the B-state can be visualized in Tn-free Ac:Tm filaments in some negative-stain reconstructions, including those reconstituted with Tm derived from both cardiac and gizzard muscle [31].

In the closed state ("C"), myosin binding to Ac:Tm(:Tn) is weak but cooperative [32,33]. According to the structural interpretation of the C-state, also inferred from negatively stained filaments, Tm shifts from its B-state position across the surface of F-Actin through a 25° rotation around the F-Actin axis to partially expose the previously buried myosin binding site [22,30]. In solution, this state is 80% occupied both in Ac:Tm filaments and Ac:Tm:Tn filaments with Ca^{2+} [26].

In the open state ("M"), myosin binding to Ac:Tm(:Tn) is strong and cooperative. According to the structural interpretation of the M-state, this position is marked by further azimuthal movement of Tm from its C-state position, through a rotation of 10° around the F-Actin axis and across the F-Actin surface, coupled to an axial shift along the F-Actin helical axis to fully expose myosin binding sites on F-Actin [23]. From the B-state to the M-state, this represents a 23-Å shift up and across with a 31° rotation around the F-Actin axis [34]. In solution, the M-state is 20% occupied in both Ac:Tm filaments and Ac:Tm:Tn filaments with Ca^{2+}, even without any myosin binding [26].

The mechanism for how the Tm filament cooperatively moves across F-Actin has remained an intriguing question ever since this three-state model and its physical interpretation, inferred from negatively stained three-dimensional electron microscopy (3DEM) structures, were proposed. Possible mechanisms have contradicting experimental support that is not always resolved by the lower-resolution negative-stain structures. Do the Tm filaments roll or shift [35,36]? Does the Tm filament act as a stiff rod or as a continuously flexible strand [17,37]? Clarification of the mechanism for Tm movement on F-Actin provides a context for understanding regulation of cardiac and smooth muscle contraction and the linkage between polymorphisms of Tm and F-Actin and disease.

Here, we show the cryo-EM structures of Ac:Tm filaments reconstituted with either bovine cardiac muscle- or chicken gizzard muscle-derived Tm that corresponds to the C-state position. By comparing the two data sets, we show that the Tn-dependent cardiac Tm reconstitutes with F-Actin into a less ordered filament than the Tn-independent gizzard Tm. From the 8-Å-resolution gizzard Tm-containing Ac:Tm structure, we propose a novel, rocking mechanism that transitions Tm from the C- to the M-state position and discuss the details about how the C-state position blocks myosin binding.

Results

Cryogenic 3DEM imaging of Ac:Tm

Ac:Tm filaments reconstituted from either bovine cardiac striated muscle-derived Tm or chicken gizzard smooth muscle-derived Tm, both assembled on F-Actin derived from rabbit skeletal muscle, were

(a)

```
G. gallus gizzard α-Tm MDAIKKKMQMLKLDKENALDRAEQAEADKKAAEERSKQLEDELVALQKKLKGTEDELDKYSESLKDAQEKL 71
G. Gallus gizzard β-Tm MEAIKKKMQMLKLDKENAIDRAEQAEADKKQAEDRCKQLEEEQQGLQKKLKGTEDEVEKYSESVKEAQEKL 71
B. taurus cardiac α-Tm MDAIKKKMQMLKLDKENALDRAEQAEADKKAAEDRSKQLEDELVSLQKKLKATEDELDKYSEALKDAQEKL 71
                      *:****************:********** **:*.****:*  .******.****::****::*:*****

G. gallus gizzard α-Tm ELADKKATDAESEVASLNRRIQLVEEELDRAQERLATALQKLEEAEKAADESERGMKVIENRAQKDEEKME 142
G. gallus gizzard β-Tm EQAEKKATDAEAEVASLNRRIQLVEEELDRAQERLATALQKLEEAEKAADESERGMKVIENRAMKDEEKME 142
B. taurus cardiac α-Tm ELAEKKATDAEADVASLNRRIQLVEEELDRAQERLATALQKLEEAEKAADESERGMKVIESRAQKDEEKME 142
                      * *:*******::**************************************************.** *******

G. gallus gizzard α-Tm IQEIQLKEAKHIAEEADRKYEEVARKLVIIEGDLERAEERAELSESQVRQLEEQLRIMDQTLKALMAAEDK 213
G. gallus gizzard β-Tm LQEMQLKEAKHIAEEADRKYEEVARKLVVLEGELERSEERAEVAESRVRQLEEELRTMDQSLKSLIASEEE 213
B. taurus cardiac α-Tm IQEIQLKEAKHIAEDADRKYEEVARKLVIIESDLERAEERAELSEGKCAELEEELKTVTNNLKSLEAQAEK 213
                      :**:**********:**************::*.:***:*****::*.:  : ***:*:: :.**:* *  ::

G. gallus gizzard α-Tm YSQKEDKYEEEIKVLTDKLKEAETRAEFAERSVTKLEKSIDDLEEKVAHAKEENLNMHQMLDQTLLELNNM 284
G. gallus gizzard β-Tm YSTKEDKYEEEIKLLGEKLKEAETRAEFAERSVAKLEKTIDDLEESLASAKEENVGIHQVLDQTLLELNNL 284
B. taurus cardiac α-Tm YSQKEDKYEEEIKVLSDKLKEAETRAEFAERSVTKLEKSIDDLEDELYAQKLKYKAISEELDHALNDMTSI 284
                      ** **********:* :*****************:****:*****:.:   * :   : : **::* ::..:
```

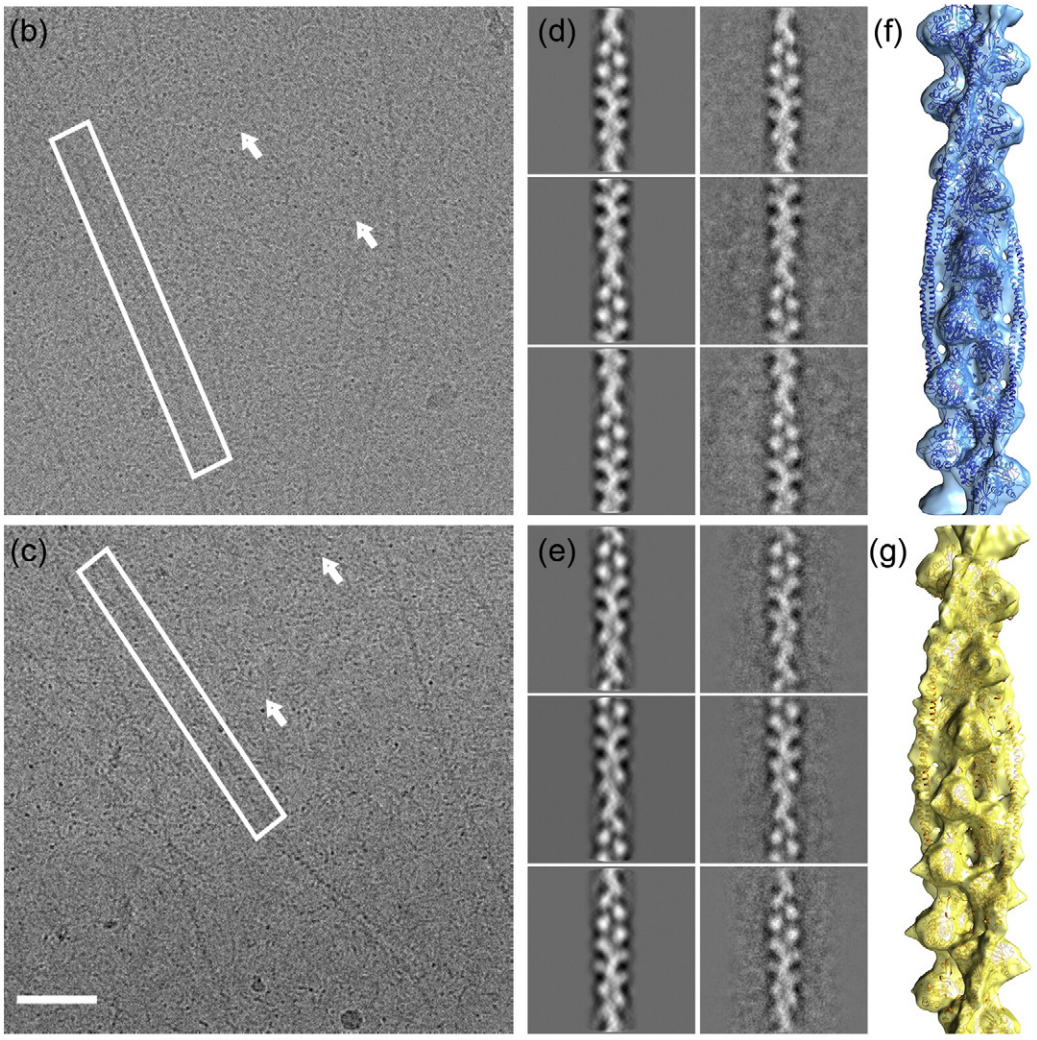

Fig. 1. Imaging Ac:Tm reconstituted with Tm derived from cardiac tissue and Tm derived from gizzard tissue. (a) Sequence alignment of the *Gallus gallus* (chicken) gizzard α and β Tm with *Bos taurus* (cow) α Tm. Identity is marked with an asterisk (*), homology is marked with a colon (:), and similarity is marked with a period (.). The heptad repeat is marked with alternating underlines. (b) Representative raw image of cardiac Ac:Tm filaments shows long, flat filaments (white box) as well as short, punctate molecules that correspond to unbound cardiac Tm molecules (white arrows). (c) Representative raw image of gizzard Ac:Tm filaments shows similar filaments (white box) and free Tm (white arrows). (d) Representative projection and corresponding class average of the cardiac Tm-containing Ac:Tm filaments. (e) Representative projection and corresponding class average of the gizzard Tm-containing Ac:Tm filaments. (f) Reconstruction of the cardiac Tm-containing Ac:Tm filament. (g) Reconstruction of the gizzard Tm-containing Ac:Tm filament.

visualized under native, cryogenic conditions (Fig. 1). Incubating a 10-fold molar excess of Tm over F-Actin allowed stable binding during the vitrification process (Fig. 1b and c). This ratio of Tm to Ac results in full binding in solution [38,39] and is similar to the Ac:Tm ratio used in imaging the recently determined high-resolution structure of Ac:Tm bound to the S1 fragment of myosin (the Behrmann model of Ac:Tm:S1) [34].

Heterogeneity

Iterative helical real space reconstruction was used to align, classify, and reconstruct structures of both isoforms. The resulting initial reconstructions, at about 20 Å resolution, reveal the Tm to be in a similar position to the C- and M-state positions, which are quite close to one another and thus difficult to distinguish at moderate resolution (Fig. 1f and g) [22]. Further, biochemical data suggest that Tm is in equilibrium between the C- and M-state positions in solution, so one possibility that could explain the moderate resolution is that there is underlying structural heterogeneity in the sample [26].

To test the hypothesis that our structure represents a mixture of Tm positions on F-Actin, we used competitive alignment against a mixed set of references for assessing heterogeneity in each data set. Both data sets were aligned against projections of five different models: bare F-Actin; the M-state Ac:Tm generated by superimposing a 14-Ac-long F-Actin and two full-length Tms from the B-state position [34] onto the shorter Ac:Tm:S1 model [Protein Data Bank (PDB) code: 4A7F [34]]; C-state Ac:Tm, generated by docking a 14-Ac-long F-Actin and two full-length Tms from the B-state position [40] into the gizzard Tm-containing Ac:Tm structure; the B-state from the atomic coordinates determined from the negative-stain structure [40]; and a noisy cylinder of diameter 7 nm (Fig. 2, row 1). Segments segregated into each model at about the same frequency but favoring the spatially similar M- and C-state positions (Table 1 breaks down the number of segments and the corresponding percentage of data that sort with each of the five models for both data sets).

Next, each subset of data was aligned against a bare F-Actin and reconstructed. In the case of the cardiac muscle-derived Ac:Tm data (Fig. 2, row 2), the 16% of filament segments that segregated with the bare F-Actin refined to produce filaments with no bound Tm. The remaining data, when aligned against the bare F-Actin model, resulted in Tm-decorated filaments where the Tm is in the C-state position, even if poorly defined for some subsets. In the case of the gizzard muscle-derived Tm data (Fig. 2, row 3), each of the subsets refine to the C-state position seen in the original refinements, visible in the raw maps.

Table 1. Mutireference alignment against diverse Ac:Tm filament models divides the single-particle segments into almost evenly distributed subsets of data.

	Cardiac, *n* (%)	Gizzard, *n* (%)
F-Actin	23,795 (16)	73,773 (15)
M-state	31,718 (22)	108,849 (23)
C-state	30,424 (21)	106,326 (22)
B-state	34,876 (24)	114,587 (24)
Cylinder	24,139 (17)	76,982 (16)

Cardiac-derived Tm

The data from the cardiac Tm-containing Ac:Tm filaments that had bound Tm were separated from the rest and further refined, resulting in a structure whose Tm is clearly shifted axially around the F-Actin, away from the B-state position defined by negative-stain 3DEM (Fig. 3). The relatively small data set results in a moderate-resolution structure, limiting the precision with which the Tm can be fit into the density axially (Figs. 3 and S1). Regardless, the azimuthal Tm position is clear. Further, there is sufficient detail to see Tm in single filament reconstructions and to ascertain the polarity of the filaments (Fig. S2), showing that the azimuthal shift that is apparent in the refined structure accurately represents the position of the Tm in the portion of the data with bound, well-ordered Tm.

Gizzard-derived Tm

Data from the gizzard Tm-containing Ac:Tm filaments showed that, unlike the cardiac-derived Tm-containing Ac:Tm, all of the filaments had bound Tm that appeared to be in the C-state position (Fig. 2). Correspondence analysis of the members of each reference-based class average, followed by subclassification and averaging, was independently performed to reduce the effects of misalignment in the final reconstruction. After classification and averaging, only the subclasses with the highest correlation to the initial reprojection were used in the final reconstruction. In this way, the amount of data was reduced from 483,139 segments (used for the initial reconstruction and Multi Reference Alignment) to 224,337 segments. Reconstruction of the classes not used for the final structure did not show heterogeneity, as expected from the MRA analysis (Fig. S3). Reconstruction of the best data improved the Fourier shell correlation resolution by about 5 Å and resolved structural details in both the F-Actin and Tm such that the Tm can be positioned both axially and azimuthally into the contours of the twisting ribbon of density that corresponds to the Tm (Fig. 4a). Only slight adjustment to the F-Actin secondary structural elements was required to accommodate the density (Fig. 4b).

pH

Next, we tested the effect of pH similar to that of uranyl formate or acetate stains to judge the potential

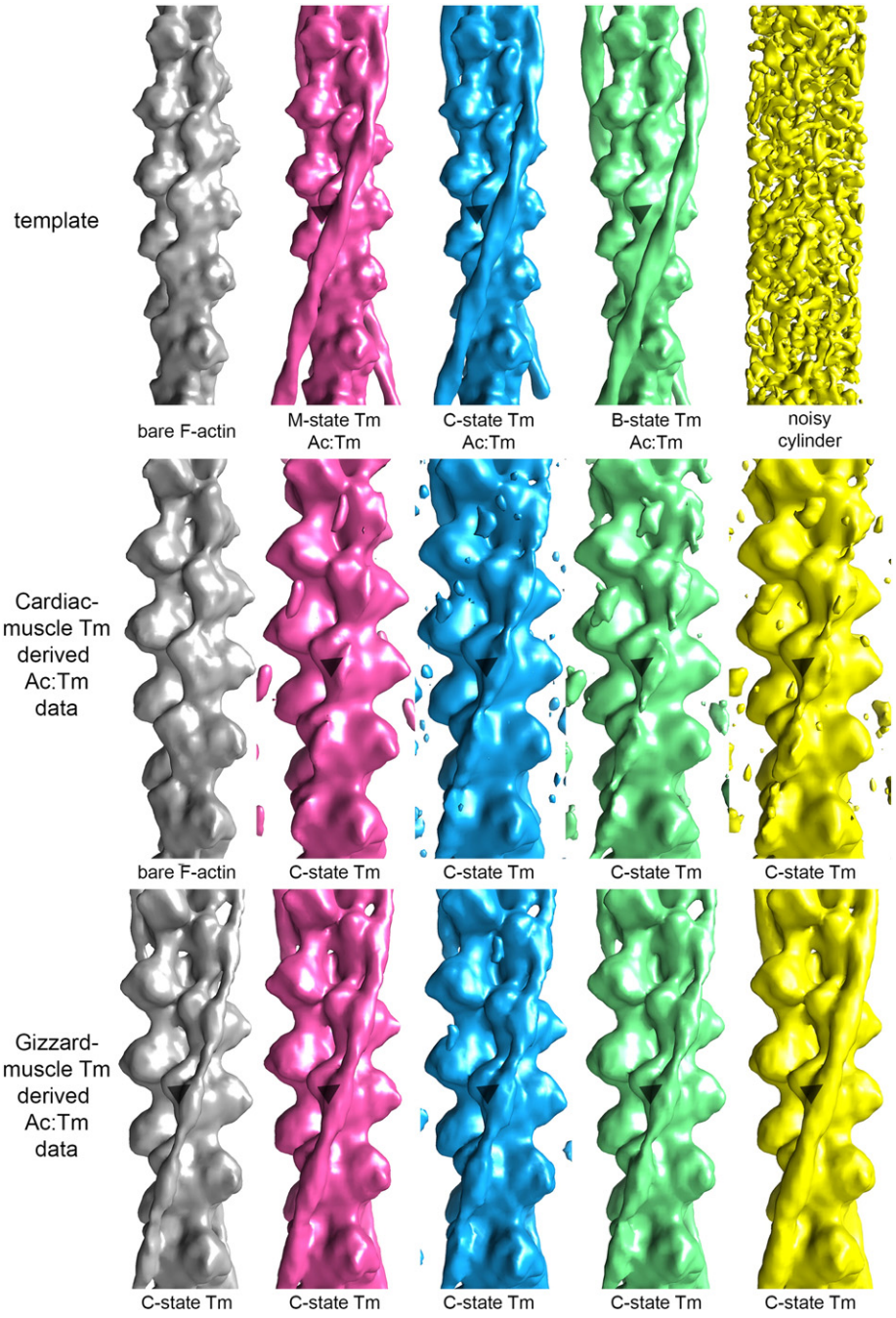

Fig. 2. Multi-reference alignment reveals that the cardiac-derived Tm-containing Ac:Tm filament is less occupied than the gizzard-derived Tm-containing Ac:Tm filament. Top row: template used for projection matching alignment. Each column represents the structure that resulted by aligning the subset of data that segregated with each model against a bare F-Actin reference. Middle row: Alignment of cardiac-derived Tm-containing Ac:Tm images that segregate with the various models show that the filaments are bare (first and last column), in the C-state and well ordered (second column), or in the C-state and not well ordered (third and fourth column). Bottom row: Alignment of gizzard-derived Tm-containing Ac:Tm images that segregate with the various models show that the majority of the filaments are occupied with C-state Tm. The arrowheads demark similar positions on the Ac to help visualize the transition of the Tm.

for artifacts in the negative-stain structures to which these cryogenic structures would be compared [31]. Both G-Actin and Tm are acidic proteins whose interaction is controlled primarily by electrostatics [40]. The p*I* of G-Actin is about 5.4 [41], whereas the p*I* of Tm is about 4.0 [42]. Their assembly is, of course,

sensitive to salt and pH [31]. To test the effect of pH on the structure of the Ac:Tm filament, we attempted to determine the cryogenic structure of a low-pH, vitrified filament. Immediately before blotting and plunging preformed Ac:Tm into ethane to preserve the filaments for cryogenic data collection, the pH of the solution was dropped by addition of a small amount of NaH_2PO_4. Rather than finding nicely spaced individual filaments, as with the pH 7 specimen (Fig. S4a), the filaments were bundled (Fig. S4b) such that they were unsuitable for single-particle helical analysis.

Discussion

Structural details of the gizzard-derived Tm-containing Ac:Tm filament

A model of a five-subunit long F-Actin and two dimeric Tm coiled coils (PDB code: 4A7F) [34], with each element docked separately, fit into the major structural elements of the F-Actin well and line up with the clear twist of the Tm (Fig. 4a). Delineated features correspond to the inner-domain helices 5, 6, 7, 8a/b, and 11, which all orient to the center of the helix, as well as the outer-domain DNase I-binding loop and adjacent helix 1, which bridge between subunits along the helix (Fig. 4b). The bulk of these elements are in the same orientation as they are when the myosin S1 domain binds (Fig. 4c). One inner-domain feature, helix 7, pivots by 10°. Likewise, the outer-domain features are slightly mismatched—the DNase I-binding loop and helix 1 are slightly out of the density, as if they should be drawn over toward the Tm. Moving those elements into the density requires only slight adjustments to the shape of the loop and orientation of the helix; these elements of the structure are variable, even when no Tm [43,44] is bound or Tm and myosin are bound [34].

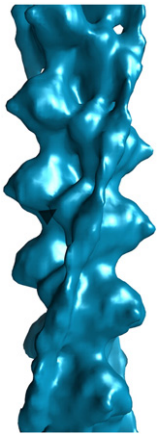

Fig. 3. Cardiac-derived Tm-containing Ac:Tm. Refinement of the occupied filaments results in a moderate-resolution structure of the C-state Ac:Tm filament.

The width and contour of the density corresponding to Tm agree well with the expected oblong shape and unambiguously show the azimuthal position of the coiled coil (Fig. 4a). The C-state position here is about 15 Å away from the M-state position, measured by the tmArg187 C^{α}–C^{α} distance between the Tm docked into the Ac:Tm or Ac:Tm:S1, where the adjacent F-Actins are superimposed. Arg187 was chosen as a good point of measurement because it is one of two amino acids identified in the Ac:Tm:S1 structure as a possible contact point with F-Actin, with acAsp311 (tmGlu181 is the other, interacting with acLys315) [34].

C-state position

The thin filament transmits stress in muscle fibers when myosin binds, hydrolyzes ATP, and changes conformation to elicit the power stroke [45]. This process is regulated by elements in the cell that sense and respond to cellular Ca^{2+} concentration to activate muscle contraction. Biochemically, three states of the thin filament serve as a framework for understanding how the proteins work together. According to this three-state steric blocking model of thin filament regulation, Tm is in equilibrium between different states that correspond to its three physical positions on F-Actin. In the absence of other regulators or in the presence of Tn and Ca^{2+}, the equilibrium is between the C- and M-states, in which myosin binds weakly and strongly, respectively [26].

Negative-stain 3DEM has provided a physical framework for understanding the Tm position corresponding to each of the three biochemical states. According to these structures, Tm moves azimuthally across the F-Actin surface from a position where it blocks myosin binding to where the myosin site is fully exposed [22]. The fully blocked position is only populated when Tn (in the absence of Ca^{2+}) pins it in place [26]. Within the confines of the three-state model, as defined by the negative-stain Ac:Tm structures, one would expect to find Tm in either the C- or the M-state position according to the equilibrium constant, which predicts they would be in a 4:1 ratio (80% closed, 20% open) [26]. The structures presented here, determined from cryogenically preserved Ac:Tm filaments, contribute structural details to this model and two competing mechanisms for the transition from the C- to the M-state.

Differences between Tm isoforms

Tm's density is sufficiently well resolved to unambiguously identify the rotation around the F-Actin helical axis in both the cardiac Tm- and gizzard Tm-containing Ac:Tm filaments, which places the Tm helical coiled coil essentially in the same location in both isoforms, when

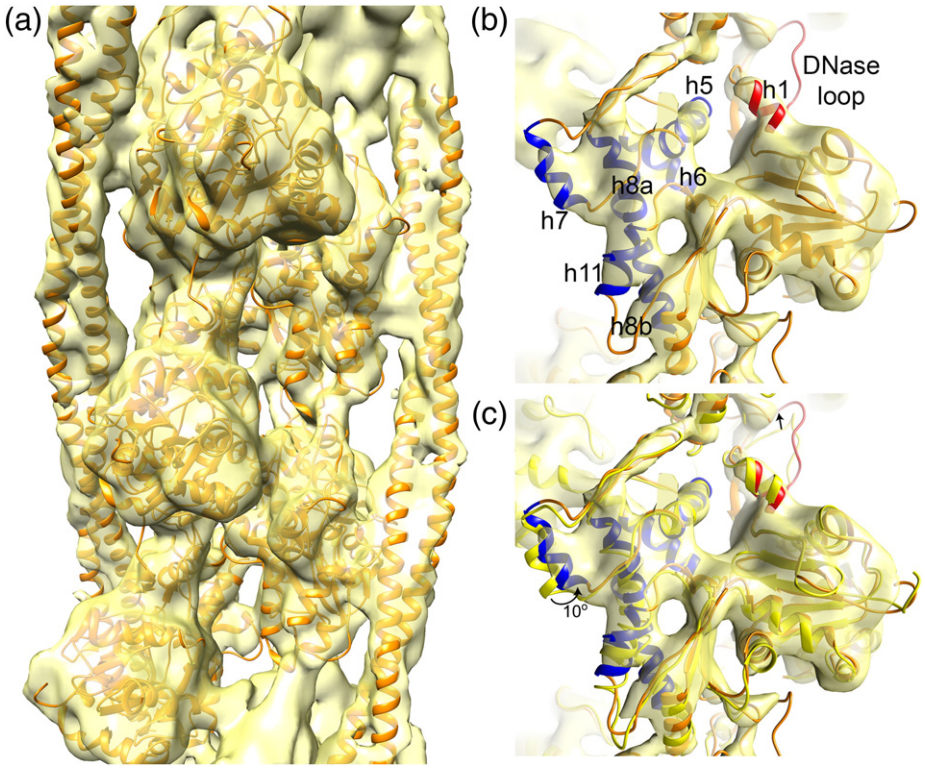

Fig. 4. Gizzard-derived Tm-containing Ac:Tm. (a) At 8 Å resolution, separation of the α-helices in the Ac and Tm is evident, allowing the independent fitting of F-Actin and Tm from Ac:Tm:S1 (PDB code: 4A7F) [34]. (b) At high contour, helices corresponding to the internal features of F-Actin are evident, showing a slight mismatch of helix 7. Helices corresponding to the inner domain (subdomains 3 and 4) are blue and those corresponding to the outer domain (subdomains 1 and 2) are red. (c) Flexible fitting rotates helix 7 by about 10° from where it sits when the myosin S1 fragment is bound (yellow).

Tm is bound (Fig. 1). Analysis of the individual segments that went into each reconstruction showed that about 15% of the cardiac-derived Tm-containing Ac:Tm filaments is undecorated, and in many of the subclasses, the Tm is poorly resolved, limiting the resolution of the resulting structure (Figs. 2, 3, and S1; Table 1). In contrast, the majority, if not all, of the gizzard-derived Tm-containing filaments were bound with Tm that wraps around F-Actin in the same, well-resolved C-state position (Fig. 2 and Table 1). Given that the filaments were prepared in the same way, the difference in filament composition is likely due to the different roles these proteins play in the cell.

Cardiac and gizzard muscle work differently in the cell; thus, it is not surprising that they behave differently biochemically and structurally. Tm is the gatekeeper of myosin activation in both muscle types regardless of Tn dependence, but despite strong sequence conservation, Ac:Tm works with different protein partners to effect change (Fig. 1a) [9,10]. It is possible that the Ac:Tm filament formed from cardiac-derived Tm and skeletal-derived F-Actin is less well ordered than that formed from gizzard-derived Tm and skeletal-derived F-Actin because it is lacking Tn, which pins it in the B-state position in the absence of Ca^{2+}. Smooth muscle, in contrast, does not need Tn so it is held in the C-state position only by interactions between F-Actin and Tm. The C-terminal regions of the sequence show the highest sequence variation between the two isoforms, pointing to the last three heptad repeats as the region of the structure that could modulate this response (Fig. 1a); the amino-terminal end of the TnT subunit also binds along the C-terminal end of Tm [46], supporting the idea that this region of the highly repetitive Tm structure is responsible for its differential regulation between isoforms.

Different behavior of Tm isoforms prepared on skeletal F-Actin has been observed [31] but has not been characterized in terms of Tm occupancy. Here, we show that Ac:Tm filaments reconstituted from gizzard (i.e., smooth) muscle-derived Tm are more occupied by Tm than that from cardiac-derived Tm (i.e., striated), suggesting differential binding affinities between isoforms that correlate with Tn dependency. The Tn-independent isoform more fully occupied by Tm and the images can be better aligned, leading to a more detailed structure, even when normalized for particle

number (Figs. 3, 4, and S1). Further, if the ability to align particles is a proxy for structural rigidity, this result would suggest that Ac:Tm filaments formed from components that do not rely on Tn, like the gizzard-derived smooth muscle Tm, are more ordered than those that rely on Tn, like the cardiac-derived striated muscle Tm, when Tn is not present.

Alternative mechanisms could explain the movement of Tm

Tm is surprisingly agile in the positions it can accommodate on the surface of F-Actin. In the C-state reported here, Tm sits over 25 Å away from where it sits in the B-state position reported from negative-stain structures [40], measured by the C^{α}–C^{α} distance between the two equivalent tmArg178 when the adjacent Ac monomer is superimposed (Fig. 5a). This represents a shift across the face of the F-Actin of about 25 Å with a rotation of 22° around the helical axis (Fig. 6b). By this same measurement, from the B-state to the M-state, Tm moves about 21 Å, shifting across the face of the F-Actin with a rotation of 28° around the helical axis measured in the same way as for the C-state position (the reported values are 23 Å shift and 31° rotation [34]). If these three positions represent a transition of Tm during myosin binding during which the same face of Tm remains in contact with F-Actin at all times, then Tm moves from the B-state position, across and around the face of the F-Actin to the C-state position, and then settles back into the M-state position with another shift of about 15 Å coupled to a 6° rotation when myosin binds (Fig. 5). Measurements involving the B-state position assume an accurately determined B-state position. Persistence length measurements define Tm as a semi-rigid rod that would more easily slide than roll, supporting this mechanism for Tm movement across the face of F-Actin [16–18]. On the other hand, fluorescence measurement shows that some amino acids believed to form the F-Actin:Tm interface are differentially solvated in the Tn – Ca^{2+} state (presumably the B-state) compared with the Tn + Ca^{2+} state (presumably the C-state), suggesting a change in the Tm environment upon repositioning that could arise if the Tm rolls by 90° around the filament [35]. Both sets of experiments deal primarily with the larger transition from B- to C-state position, implying, but not directly addressing, details about the mechanism of the smaller change from C- to M-state positions.

The transition from C- to M-state positions, defined by two reconstructions (one described in this article and the other from the Ac:Tm:S1 structure [34]), each at about 8 Å resolution, shows the possibility of a different path that requires much less movement across the F-Actin surface than a slide of 15 Å through a path almost parallel to the F-Actin axis. In both the Ac:Tm and Ac:Tm:S1 structures, the separation of the helices in the Tm is visible; hence, the coils can be placed precisely (Fig. 4). In both, a short stretch of the Tm, about five turns of one α-helix that makes up the Tm dimer, interacts with F-Actin (Fig. 6a). In the

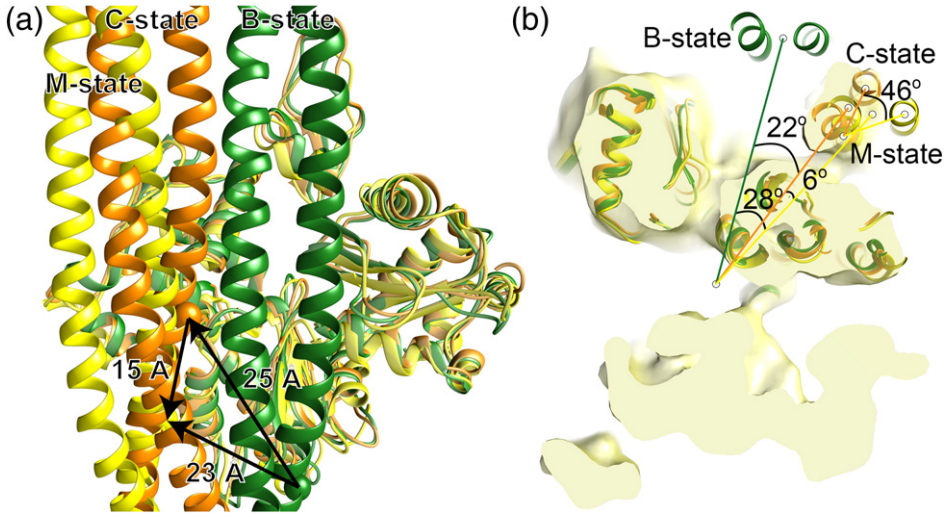

Fig. 5. B- to C- to M-state transition. (a) Tm in the C-state position (orange) is about 25 Å across the face of F-Actin from where it is in the B-state position (yellow), measured from crossover to crossover. It is about 15 Å away from where it is in the M-state (yellow), also measured from crossover to crossover. M-state Tm is about 23 Å away from B-state Tm. (b) Tm rotates 22° around the central axis of F-Actin to transition from the B- to the C-state position (green and orange, respectively) and then it rotates another 6° to move into the M-state position (yellow). A single Tm helix in the C- and M-state position is superimposable at the F-Actin interface. To move from the C- to the M-state position, the other helix rotates about 46° around that common position.

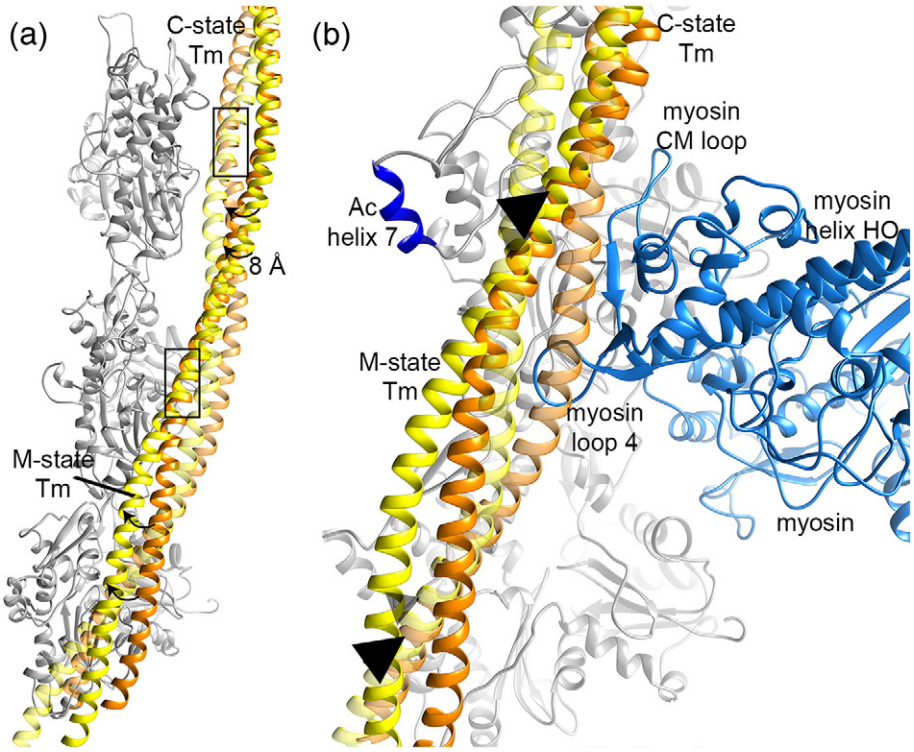

Fig. 6. Tm could rotate around a fixed position to move from the C- to the M-state. (a) When C-state Tm (orange) and M-state Tm (yellow) are independently docked into superimposed maps, a stretch of F-Actin-bound helix aligns in register, marked by a rectangle, suggesting that Tm could transition from the C- to the M-state through a rotation around this common element. (b) In the C-state (orange), steric conflict between myosin loop 4 (light blue) and the Tm helix that is not bound to F-Actin would prevent tight myosin binding. Triangles mark the overlapping helix that could be the anchor point for a rotation that allows Tm to rock out of the way, buttressed by F-Actin helix 7 (dark blue), as it moves to the M-state (yellow).

independently docked pseudo-atomic structures, that stretch of Tm is virtually superimposed, regardless of the method of superposition (i.e., docking the maps and then the models into the maps or superimposing just the models onto one another) (Figs. 5 and 6). This superposition occurs along the length of the Ac:Tm helix, owing to the symmetrized structure, but alternating which helix of the Tm dimer interacts with the F-Actin, echoing the broken Tm symmetry enforced by applying the full symmetry of the F-Actin to the full Tm dimer.

To move from the C-state position to the M-state position, the second Tm α-helix, which is not in contact with F-Actin at that position, must rock over the first by 8 Å to move from one helical position to the other, pivoting by 46° around this short stretch of Tm that remains in place (Figs. 5b and 6). In doing so, the rest of Tm follows into its new position, ultimately shifting the position of the Tm by only a small amount (Fig. 6 and Movie). This proposed rocking would be quite different from the rolling that has been suggested as an alternative to the sliding mechanism that connects the B-, C-, and M-states [35,36] because it does not involve movement across the face of the F-Actin and, as such, requires much less bending of the semi-rigid Tm coil.

Myosin binding

As docked in the C-state position, the Tm α-helix that is not in contact with the F-Actin is in direct steric conflict with myosin. Specifically, myosin loop 4 clashes with the Tm helix that is not bound to the F-Actin (Fig. 6b). Myosin loop 4 sits at the end of helix HO and participates in closure of the 50-kDa cleft upon F-Actin binding, showing how the C-state Tm position partially blocks myosin's final transition to tightly binding Ac:Tm (Fig. 6b). Interestingly, F-Actin helix 7 is positioned just on the opposite side of Tm from the myosin binding site, at the same height along the helix as the five-helical turn segment of Tm that is common between the C- and M-states. This helix rotates about 10° away from Ac subdomain 4 upon myosin binding (Fig. 4b), as if the rocking of Tm into place for myosin binding must push it slightly out of the way. Once repositioned, F-Actin helix 7 serves as a buttress, holding Tm in place after it rocks over for participation in myosin binding (Fig. 6b).

Conclusions

We present here an 8-Å-resolution cryo-EM structure of the gizzard-derived Tm-containing Ac:Tm filament that shows Tm in the C-state position. This Tm position is recapitulated in a lower-resolution Ac:Tm reconstituted with Tm derived from cardiac muscle that shows lower occupancy of Tm, suggesting binding differences between different isoforms that do or do not incorporate Tn. For the smooth muscle, gizzard-derived Tm structure, which does not use Tn, two different mechanisms could explain the trajectory of Tm as it moves between the C- and M-state positions. In one, Tm moves across the F-Actin face from the B-state position, past its binding site in the M-state to the C-state position, and then slides back into the tightly bound configuration when myosin binds. In another, B-state slides to the C-state, where tight myosin binding is blocked by steric interactions between myosin loop 4 and Tm. Upon a slight rotation around a Tm helix that remains bound to F-Actin, Tm rocks over to facilitate myosin binding.

Methods

Ac:Tm filament preparation

Rabbit skeletal muscle F-Actin, bovine cardiac Tm, and chicken gizzard Tm were purified as described elsewhere [47]. Both samples were mixed at a ratio of 1:10 Tm binding sites on F-Actin to Tm dimers, applied to well-washed QUANTIFOIL perforated carbon grids (EMS, Hatfield, PA) that had been glow discharged for 5 s in a Solarus plasma cleaner (Gatan, Warrendale, PA), and plunged at room temperature and 100% humidity using a Vitrobot plunger (FEI, Hillsboro, OR). For low-pH experiments, 0.5 μL of 1 M NaH_2PO_4 was added to the droplet of 1:10 diluted, buffered cardiac-derived Tm-containing Ac:Tm immediately before blotting and plunging into liquefied ethane.

Imaging

Images of either cardiac or gizzard Tm-containing Ac:Tm filaments were collected with an FEI Titan Krios operating at 300 kV at 101,555× magnification that resulted in a pixel size of 1.477 Å/pixel at the specimen level. A dose rate of ~30 electrons/$Å^2$ and defocus values of 1.5–4 μm were used. Images were recorded on a 4096 × 4096 Gatan Ultrascan 4000 CCD using the Leginon automated electron microscopy package [46,49].

Image processing

A total of 145,673 segments from 728 cardiac Tm-containing Ac:Tm filaments and 483,139 segments from 2992 gizzard Tm-containing Ac:Tm filaments were selected using ImageJ [50] and Eman's Boxer [51]. The segments were aligned using Matlab (The MathWorks Inc., Natick, MA), SPIDER [52], and EMAN [51]. The contrast transfer function was estimated with the Automated CTF Estimation program [53] from Appion and corrected using EMAN [54]. The iterative helical real space reconstruction technique was used to align individual segments [55]. The classes resulting from this reference-based alignment in EMAN were subsequently subclassified into 2–7 classes based on correspondence analysis performed with the CA S function in SPIDER [52]. Only images from the best matching class that matched the reference projection were kept for the final reconstruction of the gizzard-derived Tm-containing Ac:Tm data. In the final gizzard Tm-containing reconstructions, 224,337 images were reconstructed with a 28-Å rise and 167° rotation. Only images that had well-defined Tm visible in the raw structure after MRA were used in the refinement of cardiac Tm-containing data; segments included in the final reconstruction were also subject to subclassification. For this structure, 49,318 images were reconstructed with a 28-Å rise and 167° rotation. The structures observed in the resulting reconstructions of the gizzard-derived Tm-containing Ac:Tm filaments are about 8 Å resolution, judging by Fourier shell correlation at the 0.5 criterion and by features that can be visualized in the structures (Figs. 4 and S1). A *B*-factor of −487 $Å^2$ and an 8-Å low-pass filter were applied to all maps of the gizzard Tm-containing Ac:Tm structure; all reconstructions were rendered in Chimera [56]. Flexible fitting was performed with NAMD [57].

Electron Microscopy Data Bank deposition

All reconstructions were deposited in the Electron Microscopy Data Bank with the following map codes: cardiac, EMD-5752; gizzard, EMD-5751. The coordinates with a polyalanine Tm model docked into the gizzard Ac:Tm are submitted to the PDB with the codes RCSB 160242/PDB 3J4K.

Supplementary data to this article can be found online at http://dx.doi.org/10.1016/j.jmb.2013.08.020.

Acknowledgements

The authors kindly thank Ms. Cynthia Stephan-Reyes for her assistance in particle selection and Dr. P. Bryant Chase for constructive conversations. This work was funded by an American Heart Association award to M.E.S. (#10IRG4300065) and National Institutes of Health awards to William Lehman (R37 HL036153), Roger Craig (AR034711), Larry Tobacman (HL0-63774), and S.M.S. (GM086892). W.L., R.C., and L.T. provided specimen. This work was initiated while D.R.S. was supported by a National Institutes of Health training grant (HL007224) to the Whitaker Cardiovascular Institute at Boston University (J.E. Freedman, P.I.). Molecular graphics and analyses were performed with the UCSF Chimera package. Chimera is developed by the Resource for Biocomputing,

Visualization, and Informatics at the University of California, San Francisco (supported by NIGMS P41-GM103311).

Received 10 May 2013;
Received in revised form 22 August 2013;
Accepted 23 August 2013
Available online 8 September 2013

Keywords:
actin;
tropomyosin;
cryogenic 3DEM;
thin filament;
cytoskeleton

Abbreviations used:
Tm, tropomyosin; 3DEM, three-dimensional electron microscopy; Ac, actin; PDB, Protein Data Bank.

References

[1] Perry SV. Vertebrate tropomyosin: distribution, properties and function. J Muscle Res Cell Motil 2001;22:5–49.
[2] Gunning P, O'Neill G, Hardeman E. Tropomyosin-based regulation of the actin cytoskeleton in time and space. Physiol Rev 2008;88:1–35.
[3] Yang YZ, Korn ED, Eisenberg E. Cooperative binding of tropomyosin to muscle and *Acanthamoeba* actin. J Biol Chem 1979;254:7137–40.
[4] Stewart M, McLachlan AD. Fourteen actin-binding sites on tropomyosin? Nature 1975;257:331–3.
[5] Brown JH, Zhou Z, Reshetnikova L, Robinson H, Yammani RD, Tobacman LS, et al. Structure of the mid-region of tropomyosin: bending and binding sites for actin. Proc Natl Acad Sci U S A 2005;102:18878–83.
[6] Greenfield NJ, Huang YJ, Swapna GV, Bhattacharya A, Rapp B, Singh A, et al. Solution NMR structure of the junction between tropomyosin molecules: implications for actin binding and regulation. J Mol Biol 2006;364:80–96.
[7] Moore PB, Huxley HE, DeRosier DJ. Three-dimensional reconstruction of F-actin, thin filaments and decorated thin filaments. J Mol Biol 1970;50:279–95.
[8] Lehman W, Vibert P, Uman P, Craig R. Steric-blocking by tropomyosin visualized in relaxed vertebrate muscle thin filaments. J Mol Biol 1995;251:191–6.
[9] Ebashi S, Kodama A. Native tropomyosin-like action of troponin on trypsin-treated myosin B. J Biochem 1966;60:733–4.
[10] Kamm KE, Stull JT. The function of myosin and myosin light chain kinase phosphorylation in smooth muscle. Annu Rev Pharmacol Toxicol 1985;25:593–620.
[11] Gunning PW, Schevzov G, Kee AJ, Hardeman EC. Tropomyosin isoforms: divining rods for actin cytoskeleton function. Trends Cell Biol 2005;15:333–41.
[12] Brown JH, Cohen C. Regulation of muscle contraction by tropomyosin and troponin: how structure illuminates function. Adv Protein Chem 2005;71:121–59.
[13] McLachlan AD, Stewart M. Tropomyosin coiled-coil interactions: evidence for an unstaggered structure. J Mol Biol 1975;98:293–304.
[14] Parry DA. Analysis of the primary sequence of alpha-tropomyosin from rabbit skeletal muscle. J Mol Biol 1975;98:519–35.
[15] Brown JH, Kim KH, Jun G, Greenfield NJ, Dominguez R, Volkmann N, et al. Deciphering the design of the tropomyosin molecule. Proc Natl Acad Sci U S A 2001;98:8496–501.
[16] Li XE, Holmes KC, Lehman W, Jung H, Fischer S. The shape and flexibility of tropomyosin coiled coils: implications for actin filament assembly and regulation. J Mol Biol 2010;395:327–39.
[17] Sousa D, Cammarato A, Jang K, Graceffa P, Tobacman LS, Li XE, et al. Electron microscopy and persistence length analysis of semi-rigid smooth muscle tropomyosin strands. Biophys J 2010;99:862–8.
[18] Loong CK, Zhou HX, Chase PB. Persistence length of human cardiac alpha-tropomyosin measured by single molecule direct probe microscopy. PLoS One 2012;7: e39676.
[19] Holmes KC, Lehman W. Gestalt-binding of tropomyosin to actin filaments. J Muscle Res Cell Motil 2008;29:213–9.
[20] Tobacman LS. Thin filament-mediated regulation of cardiac contraction. Annu Rev Physiol 1996;58:447–81.
[21] Brown JH. Deriving how far structural information is transmitted through parallel homodimeric coiled coils: a correlation analysis of helical staggers. Proteins 2013;81(4):635–43.
[22] Poole KJ, Lorenz M, Evans G, Rosenbaum G, Pirani A, Craig R, et al. A comparison of muscle thin filament models obtained from electron microscopy reconstructions and low-angle X-ray fibre diagrams from non-overlap muscle. J Struct Biol 2006;155:273–84.
[23] Geeves MA, Lehrer SS. Dynamics of the muscle thin filament regulatory switch: the size of the cooperative unit. Biophys J 1994;67:273–82.
[24] Huxley HE. The mechanism of muscular contraction. Science 1969;164:1356–65.
[25] Ebashi S, Kodama A. Interaction of troponin with F-actin in the presence of tropomyosin. J Biochem 1966;59:425–6.
[26] McKillop DF, Geeves MA. Regulation of the interaction between actin and myosin subfragment 1: evidence for three states of the thin filament. Biophys J 1993;65:693–701.
[27] Vibert P, Craig R, Lehman W. Steric-model for activation of muscle thin filaments. J Mol Biol 1997;266:8–14.
[28] Walsh MP, Vallet B, Cavadore JC, Demaille JG. Homologous calcium-binding proteins in the activation of skeletal, cardiac, and smooth muscle myosin light chain kinases. J Biol Chem 1980;255:335–7.
[29] Dabrowska R, Sherry JM, Aromatorio DK, Hartshorne DJ. Modulator protein as a component of the myosin light chain kinase from chicken gizzard. Biochemistry 1978;17:253–8.
[30] Xu C, Craig R, Tobacman L, Horowitz R, Lehman W. Tropomyosin positions in regulated thin filaments revealed by cryoelectron microscopy. Biophys J 1999;77:985–92.
[31] Lehman W, Hatch V, Korman V, Rosol M, Thomas L, Maytum R, et al. Tropomyosin and actin isoforms modulate the localization of tropomyosin strands on actin filaments. J Mol Biol 2000;302:593–606.
[32] Lehrer SS, Morris EP. Dual effects of tropomyosin and troponin-tropomyosin on actomyosin subfragment 1 ATPase. J Biol Chem 1982;257:8073–80.

[33] Maytum R, Lehrer SS, Geeves MA. Cooperativity and switching within the three-state model of muscle regulation. Biochemistry 1999;38:1102–10.
[34] Holthauzen LM, Correa F, Farah CS. Ca^{2+}-induced rolling of tropomyosin in muscle thin filaments: the alpha- and beta-band hypothesis revisited. J Biol Chem 2004;279:15204–13.
[35] Li XE, Lehman W, Fischer S. The relationship between curvature, flexibility and persistence length in the tropomyosin coiled-coil. J Struct Biol 2010;170:313–8.
[36] Lehrer SS, Golitsina NL, Geeves MA. Actin–tropomyosin activation of myosin subfragment 1 ATPase and thin filament cooperativity. The role of tropomyosin flexibility and end-to-end interactions. Biochemistry 1997;36:13449–54.
[37] Urbancikova M, Hitchcock-DeGregori SE. Requirement of amino-terminal modification for striated muscle alpha-tropomyosin function. J Biol Chem 1994;269:24310–5.
[38] Moraczewska J, Nicholson-Flynn K, Hitchcock-DeGregori SE. The ends of tropomyosin are major determinants of actin affinity and myosin subfragment 1-induced binding to F-actin in the open state. Biochemistry 1999;38:15885–92.
[39] Zechel K, Weber K. Actins from mammals, bird, fish and slime mold characterized by isoelectric focusing in polyacrylamide gels. Eur J Biochem 1978;89:105–12.
[40] Giometti CS, Anderson NL. Tropomyosin heterogeneity in human cells. J Biol Chem 1984;259:14113–20.
[41] Galkin VE, Orlova A, Schroder GF, Egelman EH. Structural polymorphism in F-actin. Nat Struct Mol Biol 2010;17:1318–23.
[42] Splettstoesser T, Holmes KC, Noe F, Smith JC. Structural modeling and molecular dynamics simulation of the actin filament. Proteins 2011;79:2033–43.
[43] Geeves MA, Fedorov R, Manstein DJ. Molecular mechanism of actomyosin-based motility. Cell Mol Life Sci 2005;62:1462–77.
[44] White SP, Cohen C, Phillips Jr GN. Structure of co-crystals of tropomyosin and troponin. Nature 1987;325:826–8.
[45] Tobacman LS, Adelstein RS. Mechanism of regulation of cardiac actin-myosin subfragment 1 by troponin–tropomyosin. Biochemistry 1986;25:798–802.
[46] Suloway C, Pulokas J, Fellmann D, Cheng A, Guerra F, Quispe J, et al. Automated molecular microscopy: the new Leginon system. J Struct Biol 2005;151:41–60.
[47] Shrum DC, Woodruff BW, Stagg SM. Creating an infrastructure for high-throughput high-resolution cryogenic electron microscopy. J Struct Biol 2012;180:254–8.
[48] Abramoff MD, Magelhaes PJ, Ram SJ. Image processing with ImageJ. Biophoton Int 2004;11:36–42.
[49] Ludtke SJ, Baldwin PR, Chiu W. EMAN: semiautomated software for high-resolution single-particle reconstructions. J Struct Biol 1999;128:82–97.
[50] Frank J, Radermacher M, Penczek P, Zhu J, Li Y, Ladjadj M, et al. SPIDER and WEB: processing and visualization of images in 3D electron microscopy and related fields. J Struct Biol 1996;116:190–9.
[51] Mallick SP, Carragher B, Potter CS, Kriegman DJ. ACE: automated CTF estimation. Ultramicroscopy 2005;104:8–29.
[52] Lander GC, Stagg SM, Voss NR, Cheng A, Fellmann D, Pulokas J, et al. Appion: an integrated, database-driven pipeline to facilitate EM image processing. J Struct Biol 2009;166:95–102.
[53] Egelman EH. A robust algorithm for the reconstruction of helical filaments using single-particle methods. Ultramicroscopy 2000;85:225–34.
[54] Pettersen EF, Goddard TD, Huang CC, Couch GS, Greenblatt DM, Meng EC, et al. UCSF Chimera—a visualization system for exploratory research and analysis. J Comput Chem 2004;25:1605–12.
[55] Phillips JC, Braun R, Wang W, Gumbart J, Tajkhorshid E, Villa E, et al. Scalable molecular dynamics with NAMD. J Comput Chem 2005;26:1781–802.

Supplementary data references

[34] E. Behrmann, M. Muller, P.A. Penczek, H.G. Mannherz, D.J. Manstein, S. Raunser. Structure of the rigor actin–tropomyosin–myosin complex. Cell 2012;150:327–38
[40] X.E. Li, L.S. Tobacman, J.Y. Mun, R. Craig, S. Fischer, W. Lehman. Tropomyosin position on F-actin revealed by EM reconstruction and computational chemistry. Biophys J 2011;100:1005–13
[56] Grigorieff N. FREALIGN: high-resolution refinement of single particle structures. J Struct Biol 2007;157:117–25.
[57] Pettersen EF, Goddard TD, Huang CC, Couch GS, Greenblatt DM, Meng EC, et al. UCSF Chimera–a visualization system for exploratory research and analysis. J Comput Chem 2004;25:1605–12.